Chemical Science

ROYAL SOCIETY OF CHEMISTRY

EDGE ARTICLE

View Article Online
View Journal | View Issue

Cite this: *Chem. Sci.*, 2026, **17**, 1195

All publication charges for this article have been paid for by the Royal Society of Chemistry

Received 22nd September 2025
Accepted 6th November 2025

DOI: 10.1039/d5sc07321a

rsc.li/chemical-science

A bow-like axially chiral cycloparaphenylene with simultaneously enhanced photoluminescence quantum yield and dissymmetry factor

Meng-Xue Yu,[ab] Chao Feng,[a] Wei-Chen Guo[ab] and Chuan-Feng Chen *[ab]

Cycloparaphenylenes (CPPs) with unique luminescent properties and well-defined dimensions are considered as ideal blocks for achieving excellent circularly polarized luminescence performance. Chiral CPPs face challenges in simultaneously achieving both high photoluminescence quantum yield (PLQY) and luminescence dissymmetry factor (g_{lum}) due to their unique size effects. In this work, a bow-shaped axially chiral CPP, named **4CzZ[6]CPP**, was designed and synthesized by utilizing a carbazole-modified donor–acceptor axially chiral unit through a chirality embedding strategy. The topological structure and photophysical properties were elucidated through crystallography and spectroscopy. Remarkably, **4CzZ[6]CPP** showed an exceptional PLQY of 74.4% due to the interaction charge transfer (ICT) process and the constrained conformation. In particular, the (*R*/*S*)-**4CzZ[6]CPP** exhibited a maximum $|g_{\mathrm{lum}}|$ of up to 6.43×10^{-3} because of the rigid structure, representing a 2.5-fold enhancement compared to the chiral precursors, which was confirmed by theoretical calculations. Additionally, a high circularly polarized luminescence brightness (B_{CPL}) of 344 $\mathrm{M^{-1}\ cm^{-1}}$ was achieved, which represents a new record among chiral CPPs constructed by a chirality embedding strategy reported to date.

Introduction

The unique π-conjugated electronic structure of macrocycles endows them with remarkable conformational diversity and distinctive optoelectronic properties, raising interest in supramolecular chemistry and organic functional materials.[1] The cycloparaphenylene (CPP) scaffold comprises a macrocyclic architecture formed by *para*-linked benzene units. Since Jasti and co-workers first proposed and perfected the synthetic route of CPPs,[2] they have served as versatile synthons for constructing carbon nanotubes[3] and probing host–guest complexation[4] and supramolecular assembly[5] in macrocyclic systems. In addition, CPP derivatives have gradually appeared as luminescent materials due to their well-defined dimensions, versatile functionalization and tunable fluorescence emission characteristics. However, the limited fluorescence performance of CPPs has motivated structural diversification to enable precise material design for broader applications.

In recent years, circularly polarized luminescence (CPL) has attracted increasing interest due to its potential applications in displays,[6] anti-counterfeiting encryption,[7] optical switches,[8] and biological imaging.[9] The comprehensive performance of CPL is evaluated by the circularly polarized luminescence brightness ($B_{\mathrm{CPL}} = 1/2\varepsilon \times \Phi_{\mathrm{PL}} \times g_{\mathrm{lum}}$). Imparting CPL activity to CPPs represents a promising approach to not only develop their diverse structures but also enhance their luminous performance.[10] In 2011, Isobe[11] reported a planar chiral CPP derivative, but its chiral characteristics remained unexplored. Directly embedding chiral or achiral functional groups as symmetry-breaking substructures into CPPs is a convenient and important strategy for developing chiral CPP structures. By integrating achiral units (*e.g.*, naphthalene,[12] phenanthrene,[13] perylene diimide,[14] and rubicene[15]) and chiral units[16–18] into the CPP framework, Du *et al.* constructed a series of chiral CPP derivatives with obvious chiroptical properties, but the photoluminescence quantum yields (PLQYs) remain unsatisfactory. In previous works, CPPs have been primarily regarded as simple molecular building units, with their distinctive size effect remaining largely unexplored. Recently, Jiang *et al.*[19] synthesized size-variable CPPs featuring central chirality using a trimethylene linker, revealing an inverse correlation between the g_{lum} values and PLQYs: the g_{lum} values increased while the PLQYs decreased on reducing the ring size. Notably, based on Rosenfeld's equation, $g_{\mathrm{lum}} = 4\cos\theta|m||\mu|/|m|^2 + |\mu|^2$, where μ and m represent the electric and magnetic transition dipole moments, respectively, and θ is the angle between μ and m. For chiral organic small molecules, it is a viable strategy to enhance the structural rigidity to reduce μ and to amplify the g_{lum} value.[20] However, when the size of the CPPs reduces to a certain number (typically, $n < 7$), the PLQY drops sharply due to the excessive strain.[21] To date, simultaneously achieving both high PLQYs

---

[a] Beijing National Laboratory for Molecular Sciences, CAS Key Laboratory of Molecular Recognition and Function, Institute of Chemistry, Chinese Academy of Sciences, Beijing 100190, China. E-mail: cchen@iccas.ac.cn

[b] University of Chinese Academy of Sciences, Beijing 100049, China

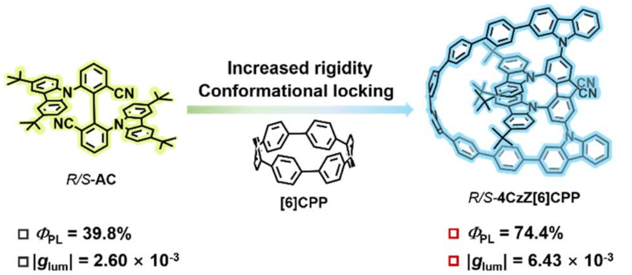

Fig. 1 Schematic diagram of the design and construction of axially chiral CPPs in this work.

and large g_{lum} values in chiral CPP derivatives by the chirality embedding strategy remains a significant challenge.

Herein, we report a donor–acceptor axially chiral CPP with a bow-like structure, named **4CzZ[6]CPP** (Fig. 1), which can be successfully synthesized by a four-step coupling reaction and one-step reduction reaction, respectively. X-ray single crystal diffraction confirms the molecular structure. The C–H⋯π interactions between the 3,6-di-*tert*-butylcarbazole and the CPP skeleton limit the molecular rotation and improve the conformational stability. Moreover, **4CzZ[6]CPP** shows a large molar extinction coefficient (ε) up to 2.2 × 10^5 M^{-1} cm^{-1} due to the large conjugated structure and displays a bright blue fluorescence peak at 458 nm in toluene and a transient lifetime of 27.6 ns in dichloromethane (DCM). As expected, the interaction charge transfer (ICT) process introduced by the donor–acceptor structure and the locked conformation enhances the PLQY with Φ_{PL} of 74.4%. In particular, both the experimental and theoretical results reveal that the incorporation of CPPs leads to a 2.5 times amplification of g_{lum} to 6.43 × 10^{-3} in toluene compared with the axially chiral monomer *R*/*S*-**AC** (Fig. 1). Consequently, a new record B_{CPL} of 344 M^{-1} cm^{-1} among the reported chiral CPPs is achieved.

Results and discussion

Synthesis and characterization

The tunable size of CPPs can adjust the luminescence properties. The rigidity of small-sized CPPs was enhanced, which provided the possibility to obtain large g_{lum} values. Axially chiral molecules are promising candidates for chiral sources with a pronounced chiral response and high enantiomer stability.[22] Additionally, the charge transfer (CT) state introduced by the donor–acceptor (D–A) structure increases radiative transition pathways. The integration of axially chiral units, featuring a D–A structure, into the CPP framework not only preserves the inherent luminescence characteristics of the CPP but also enhances the overall luminescence performance. As a result, we designed a new CPP derivative, **4CzZ[6]CPP**, with a D–A structure in the CPP framework. As shown in Scheme 1, **ClCz** was synthesized in 83% yield by a Suzuki–Miyaura coupling reaction between molecules **1** and **2**-bromocarbazole. Under the reaction conditions of using tris(dibenzylideneacetone)dipalladium as the catalyst and 1,1′-bis(diphenylphosphino)ferrocene as the ligand, **ClCz** and molecule **2** were integrated through a Buchwald–Hartwig cross-coupling reaction to obtain **2ClCzZ** in a yield of 60%. With palladium diacetate as the catalyst and 2-dicyclohexylphosphino-2′,6′-dimethoxy-1,1′-biphenyl as the ligand, the two Cl atoms were successfully converted into two borate groups in a dehydrated 1,4-dioxane solution by a Miyaura borylation reaction. Finally, the **4CzZ[6]CPP** macrocyclic precursor was obtained by the self-coupling cyclization reaction of **2BpinCzZ**. It was found that the macrocyclic precursor was

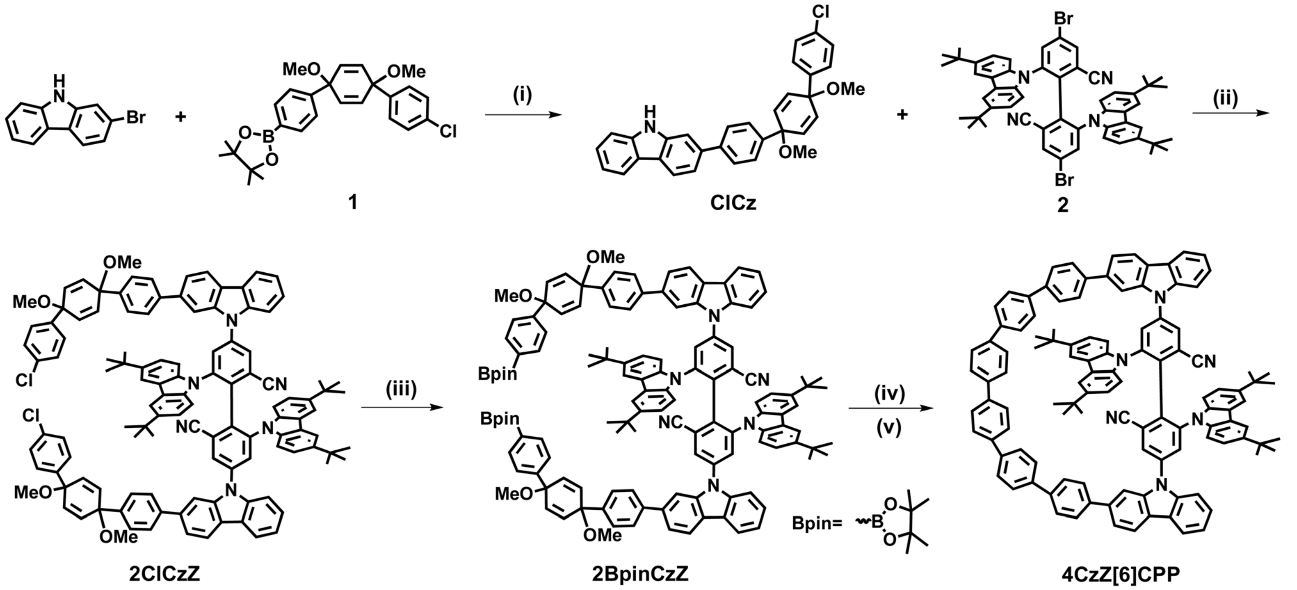

Scheme 1 Synthesis of **4CzZ[6]CPP**. (i) $Pd(PPh_3)_4$, K_2CO_3, toluene, ethanol, H_2O, reflux, 83%; (ii) $Pd_2(dba)_3$, dppf, Cs_2CO_3, toluene, 120 °C, 60%; (iii) $Pd(OAc)_2$, *S*-phos, 2-[(*tert*-butyldimethylsilanyl)ethynyl]boronic acid pinacol ester, K_3PO_4, 1,4-dixoane 90 °C, 12 h, 55%; (iv) $Pd(PPh_3)_2Cl_2$, $B(OH)_3$, KF, THF, H_2O, 40 °C, overnight; (v) H_2SnCl_4, THF, 25 °C, 6 h, 12%.

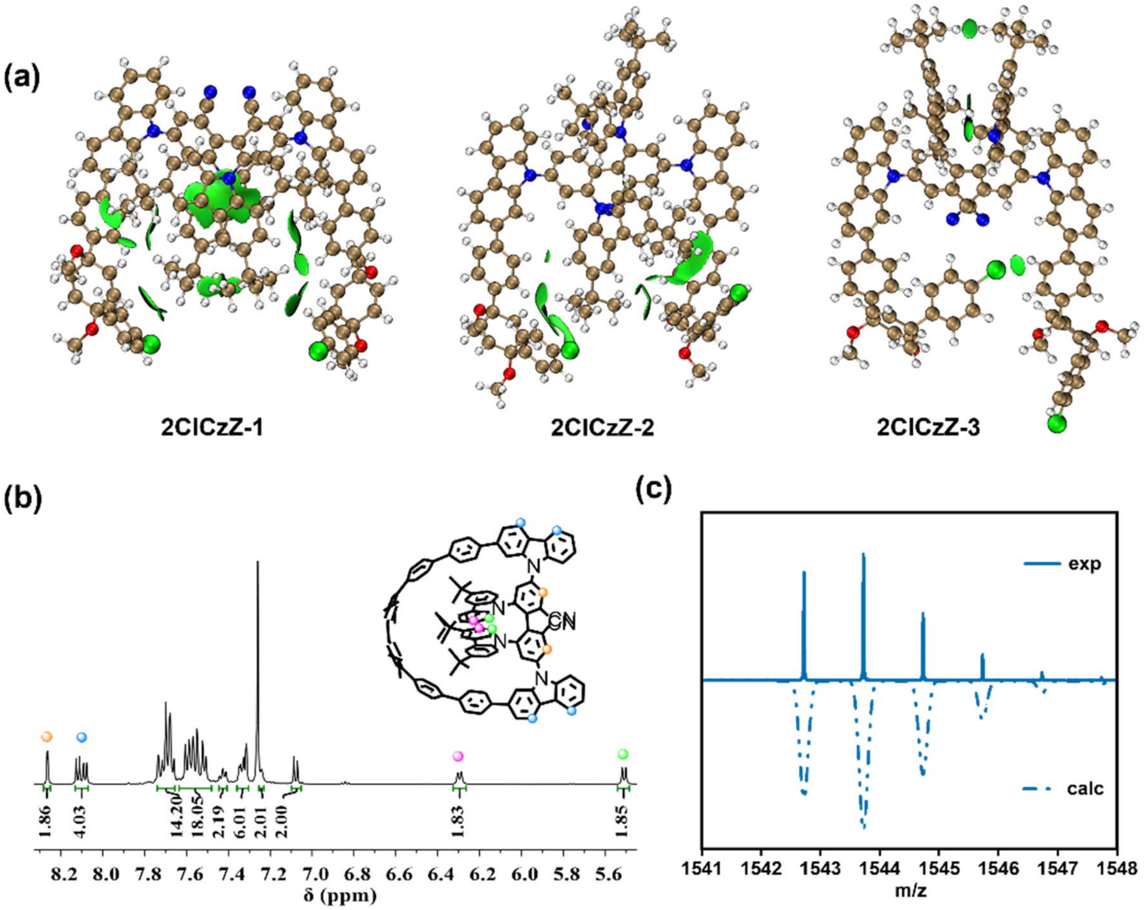

Fig. 2 (a) IGMH analysis of 2ClCzZ-1, 2ClCzZ-2 and 2ClCzZ-3. (b) The ^{1}H NMR and (c) mass spectrum of 4CzZ[6]CPP.

unstable in solution; therefore, it was promptly converted to the target product **4CzZ[6]CPP** by reductive aromatization under mild conditions. The total yield of the cyclization reaction and reductive aromatization reaction was 12%. All molecules were separated and purified by column chromatography and then structurally characterized using ^{1}H NMR, ^{13}C NMR and high-resolution mass spectra (HRMS) (Fig. S1–S7). The peaks of the experiment at $m/z = 1542.7223$ and theoretical results were consistent, confirming the successful synthesis of **4CzZ[6]CPP** (Fig. 2c). In addition, we found that **4CzZ[6]CPP** exhibited high stability in an air atmosphere.

Structural analysis

In the ^{1}H NMR spectra, the aromatic protons of **2ClCzZ** and **2BpinCzZ** exhibited an unusual up-field shift ($\delta = 5.7$ ppm), suggesting potential weak interactions between the CPP fragment and 3,6-di-*tert*-butylcarbazole. This phenomenon could be attributed to the preorganized arrangement of the 3,6-di-*tert*-butylcarbazole moieties and the shielding effect of the π-conjugated structure. Following cyclization to form **4CzZ[6]CPP**, these protons experienced further shielding ($\delta = 5.5$ ppm), demonstrating enhanced intra-annular magnetic anisotropy in the constrained macrocyclic system. Theoretical analysis of **2ClCzZ** revealed three distinct conformations differing in the carbazole orientation, named **2ClCzZ-1**, **2ClCzZ-2** and **2ClCzZ-3**, respectively. The independent gradient model based on Hirshfeld partition (IGMH) was performed to identify significant weak interactions between the 3,6-di-*tert*-butylcarbazole and CPP unit (Fig. 2a). The results indicated C–H⋯π interactions between both 3,6-di-*tert*-butylcarbazole units and the CPP fragment, alongside π–π stacking between the two 3,6-di-*tert*-butylcarbazole moieties in **2ClCzZ-1**, only one 3,6-di-*tert*-butylcarbazole engaged the CPP fragment *via* C–H⋯π interaction in **2ClCzZ-2** and exclusive π–π stacking was observed between the two 3,6-di-*tert*-butylcarbazole groups in **2ClCzZ-3**. Gibbs free energy calculations showed that conformers **2ClCzZ-2** and **2ClCzZ-3** exhibited comparable energies, whereas **2ClCzZ-1** is energetically stabilized by 11.321 and 9.437 kcal mol^{-1} relative to **2ClCzZ-2** and **2ClCzZ-3**, respectively (Fig. S34). These results confirmed **2ClCzZ-1** as the thermodynamically preferred configuration, which was consistent with our experimental observations. Based on the preference of substrate configuration and the COSY and NOESY spectra (Fig. S8 and S9), we performed a preliminary assignment of the characteristic hydrogen atoms in **4CzZ[6]CPP** (Fig. 2b).

Single crystals of **4CzZ[6]CPP** suitable for X-ray diffraction were successfully obtained through slow diffusion of CH_3CN into a $CHCl_3$ solution. The obtained crystal structure revealed a well-defined bow-shape conformation (Fig. S12). The molecular structure exhibited remarkable dimensions with an arm length of 14.35 Å and a bowstring length of 12.87 Å (Fig. 3a). Crystallographic analysis confirmed that **4CzZ[6]CPP** crystallized in the triclinic P_1 space group, possessing no symmetrical element except for the C1 symmetry (Table S1). Each crystal cell contained a pair of enantiomers, with the *S*-configuration displaying distinct structural features: (1) the upper carbazole moiety twisted outward by 23°, and the lower carbazole twisted inward by 52°; (2) the directly connected benzene (A and B) maintained near-parallel alignment (5° dihedral angle); (3) the adjacent benzene exhibited substantial torsional angles of 79° and 73°, respectively, creating a highly distorted Möbius-like conformation. The molecular chirality originated from a 72° torsional angle in the biphenyl unit, with the chiral character propagating efficiently through the conjugated benzene framework. Notably, intramolecular coulombic repulsion induced significant dihedral angles of 152° and 146° between the 3,6-di-*tert*-butylcarbazole and biphenyl moieties (Fig. S13). Furthermore, the inherent ring strain of the CPP framework induced a pronounced torsional distortion of 25° between the two 3,6-di-*tert*-butylcarbazoles, forcing one of the 3,6-di-*tert*-butylcarbazoles to be partially extruded from the macrocycle. Finally, C–H⋯π and π–π interactions were predominantly observed between the carbazole of the enantiomers and the adjacent benzene or 3,6-di-*tert*-butylcarbazole moieties, with intermolecular distances of approximately 3 Å (Fig. S15). Under the synergistic influence of weak noncovalent forces, *R*-**4CzZ[6]CPP** and *S*-**4CzZ[6]CPP** adopted an alternating wave-like arrangement along the *b*-axis, while a lamellar packing motif emerged along the *c*-axis (Fig. 3b). Moreover, C–H⋯π interactions between the 3,6-di-*tert*-butylcarbazole and conjugated benzene moieties within a single conformation were identified with the distance of about 2.83 Å (Fig. S14). These interactions restricted the rotation of the 3,6-di-*tert*-butylcarbazole and enhanced the conformational stability.

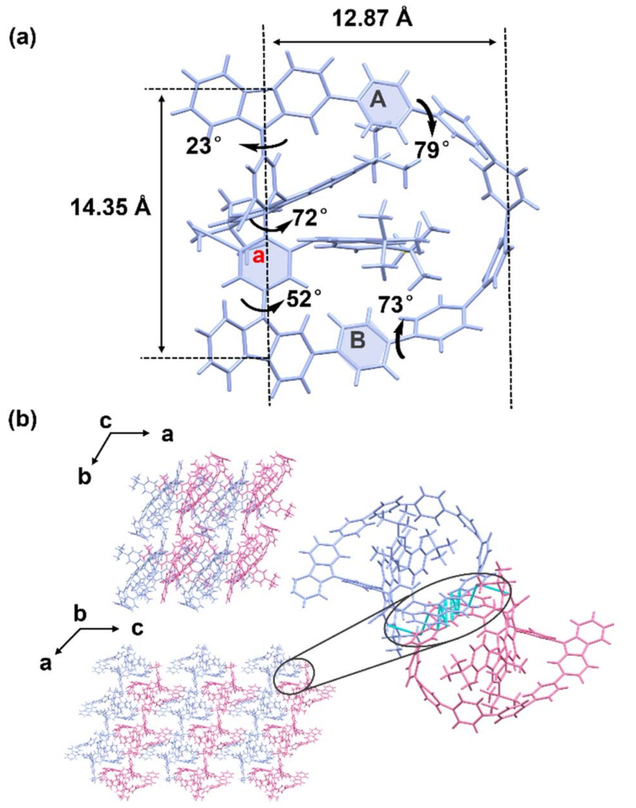

Fig. 3 (a) The single crystal structure of *S*-4CzZ[6]CPP. (b) The stacking mode from the *a* and *b*-axes directions and the weak interaction between the enantiomers of (*rac*)-4CzZ[6]CPP.

Theoretical calculations, photophysical and electrochemical properties

To gain insight into **4CzZ[6]CPP**, the electrostatic potential (ESP) map was carried out to study the electronic properties, which revealed a uniform distribution of electron density across the conjugated benzene and 3,6-di-*tert*-butylcarbazole units, while pronounced electron enrichment was observed at the cyano group due to its strong electron-withdrawing character (Fig. S36). In addition, density functional theory (DFT) and time-dependent DFT (TD-DFT) calculations were performed to study the photophysical properties of **4CzZ[6]CPP**. As shown in Fig. 4a, the highest occupied molecular orbital (HOMO) was localized on the 3,6-di-*tert*-butylcarbazole moiety, whereas the lowest unoccupied molecular orbital (LUMO) resided predominantly on the cyano group, which was consistent with the distribution characteristics of D–A molecular orbitals. The

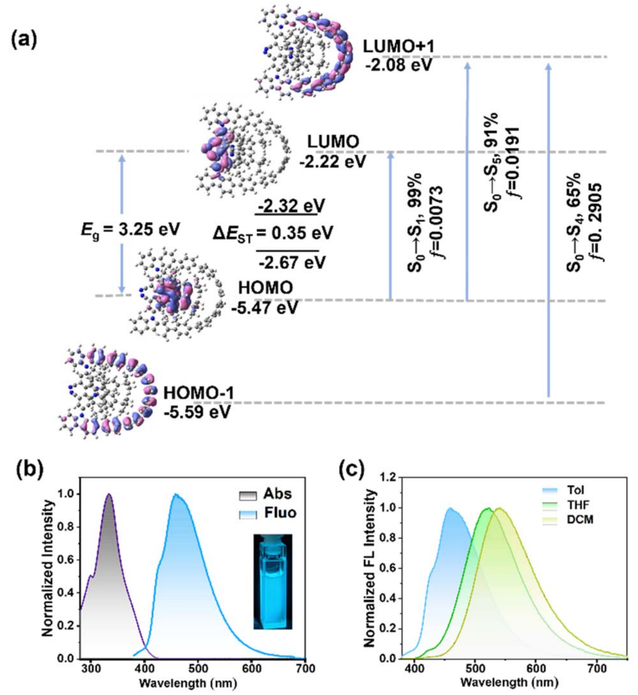

Fig. 4 (a) The energy of major molecule orbitals and the contributions and *f* values in the transition process with the B3lyp/def2svp basis group. (b) The absorption and fluorescence spectra of 4CzZ[6]CPP, and its inset photograph in toluene. (c) Solvation effect of 4CzZ[6]CPP. $c = 1 \times 10^{-6}$ M.

HOMO and LUMO energies were determined to be −5.47 eV and −2.22 eV, respectively, yielding an energy gap (E_g) of 3.25 eV. In addition, the singlet-triplet energy gap (ΔE_{ST}) was determined to be 0.35 eV. Owing to the electron-accepting nature of the conjugated benzene, the HOMO-1 and LUMO-1 orbitals exhibited delocalization on the CPP backbone in opposing spatial orientations (Fig. S35).

The UV-vis absorption and fluorescence spectra were recorded at 298 K (Fig. 4b). In toluene solution, **4CzZ[6]CPP** exhibited a dominant absorption maximum at 335 nm, characteristic of the π–π* transition within the extended π-conjugated macrocyclic framework, which was consistent with typical CPP derivatives. A weaker low-energy absorption band appeared at 373 nm, originating from a weak intramolecular charge transfer (ICT) process. Remarkably, **4CzZ[6]CPP** demonstrated an exceptionally high molar extinction coefficient ($\varepsilon = 2.2 \times 10^5\ M^{-1}\ cm^{-1}$), representing a significant enhancement over reported [6-10]CPP derivatives.[23] This improvement could be rationalized by the extended π-conjugation through multiple carbazole and cyano groups, and the optimized structural rigidity that enhanced orbital overlap. The TD-DFT results showed that the absorption peak at 344 nm was due to the electronic transition from the HOMO-1 and HOMO to LUMO+1 orbitals with the oscillator strengths (*f*) of 0.0191 and 0.2905, while the absorption peak at 373 nm was determined to be the HOMO to LUMO electronic transition with *f* of 0.0073 (Table S7). Hole–electron analysis showed that the structural relaxation indices (S_r) of these transition processes were 0.67, 0.44 and 0.27 (a.u.), respectively, which displayed large overlap between the hole and electron density distributions (Tables S8 and S9). Moreover, natural transition orbital (NTO) analysis indicated that the contribution rates of the orbital transitions from S_0 to S_1, S_2 and T_1 were 99.52%, 99.04% and 75.18%, respectively (Fig. S37). These results indicated the intense fluorescence emission. As shown in Fig. 4b, **4CzZ[6]CPP** exhibited a blue photoluminescence with the maximum peak at 458 nm in toluene, which displayed a significant blue-shift compared to the **AC** due to the multiple carbazole units (Fig. S25). Additionally, the large Stokes shift of 123 nm indicated the pronounced solvent effect. The absorption spectra of **4CzZ[6]CPP** were similar in solutions with different polarities and in films (Fig. S16, S17 and Table S2), while the maximum emission wavelengths in THF and DCM were red-shifted to 522 and 539 nm, respectively (Fig. 4c). The transient decay curve confirmed that the prompt fluorescence lifetime (τ_{PF}) of **4CzZ[6]CPP** was 27.6 ns (Fig. S18).

Afterwards, the experimental E_g of **4CzZ[6]CPP** was determined to be 2.91 eV based on the absorption spectrum at 298 K. Through cyclic voltammetry measurement under a N_2 atmosphere, we further studied the electrochemical properties (Fig. S30). The oxidation and reduction potential curves were measured in anhydrous DCM and THF, respectively. We found that the HOMO energy was estimated to be −5.48 eV, and the LUMO energy was calculated to be −2.74 eV ($E_g = E_{LUMO} - E_{HOMO}$). These results showed excellent agreement with the theoretical calculations. Additionally, compared to [6-10]CPP ($E_{HOMO} = -4.915$ to -5.198 eV),[24] **4CzZ[6]CPP** exhibited a deeper HOMO energy level, effectively suppressing non-radiative transitions, and thereby enhancing the luminescence efficiency. The photophysical and electrochemical data are summarized in Table 1.

Unexpectedly, **4CzZ[6]CPP** exhibited a high Φ_{PL} of 74.4% using an integrating sphere (Fig. S20), demonstrating that embedding a D–A axially chiral unit within [6]CPP conferred intense fluorescence relative to [6]CPP without fluorescence emission.[24] This photophysical enhancement arose from introducing moderate charge-transfer (CT) character to the D–A structure, increasing the pathways of radiative transitions, and the radiative transition rate constant (k_r) reached $2.7 \times 10^7\ s^{-1}$. In addition, compared to the lowΦ_{PL} of 39.4% in **AC** (Fig. S26), the improvement in PLQY in **4CzZ[6]CPP** originated from the conformationally locked macrocycle, which suppressed the vibrational dissipation. At the same time, the enhanced structural rigidity limited the non-radiative transition pathways. Furthermore, theoretical calculations of macrocycle strain energy revealed that **4CzZ[6]CPP** possessed a modest macrocycle strain energy of 22.04 kcal mol^{-1} (Table S10), less than the strain energies of [6-10]CPP (58–97 kcal mol^{-1}).[25] Strain energy release within the conformationally constrained [6]CPP framework also played an important role in PLQY enhancement. Additionally, the PLQY of **4CzZ[6]CPP** measured in the film state dropped to 30%, which could be attributed to strong π–π interactions in the tightly packed structure causing non-radiative transitions (Fig. S21).

Chiroptical properties

The incorporation of axially chiral luminescent molecule (*R*/*S*)-**AC** endowed (*R*/*S*)-**4CzZ[6]CPP** with pronounced chiroptical properties. The enantiomeric resolution of (*R*/*S*)-**AC** and (*R*/*S*)-**4CzZ[6]CPP** was achieved successfully *via* high-performance liquid chromatography (HPLC) and demonstrated exceptional enantiomeric excess (ee, >99%) (Fig. S31, S32 and Tables S3–S6).

Table 1 Photophysical and electrochemical properties of (*rac*)-4CzZ[6]CPP

Compound	$\lambda_{abs}{}^a$ (nm)	$\lambda_{FL}{}^a$ (nm)	$\varepsilon^a\ M^{-1}\ cm^{-1}$	$\Phi_{PL}{}^b$ (%)	$\tau_{PF}{}^b$ (ns)	$k_r{}^b$ (s^{-1})	$E_{HOMO}{}^c$ (eV)	$E_{LUMO}{}^d$ (eV)	$E_g{}^d$ (eV)
4CzZ[6]CPP	335	458	2.2×10^5	74.4	27.6	2.7×10^7	−5.48	−2.57	2.91

[a] Measured and calculated in toluene at 298 K. [b] Measured in DCM at 298 K. [c] Measured in dehydrated DCM and calculated from the oxidation curve with the formula of $E_{HOMO} = -[E_{OX} - E_{(Fc/Fc^+)} + 4.8]$ eV. [d] Estimated from the absorption spectrum and obtained using $E_g = 1240/\lambda_{onset}$, $E_g = E_{LUMO} - E_{HOMO}$.

The absolute configurations of (*R*/*S*)-**AC** and (*R*/*S*)-**4CzZ[6]CPP** were confirmed by the TD-DFT calculated electronic circular dichroism (ECD) spectrum, which established the shorter retention component as the *S*-**AC** and *S*-**4CzZ[6]CPP**, respectively (Fig. 5a and S27). The UV-vis spectra of both enantiomers of (*R*/*S*)-**4CzZ[6]CPP** were identical to that of the racemate, confirming that there is no damage to the macrocycle during chiral separation and an exceptional configurational stability under ambient conditions (Fig. S19). Furthermore, we heated *S*-**4CzZ[6]CPP** in 1,3,5-triisopropylbenzene at 220 °C for 18 h, and no racemization was induced through HPLC monitoring (Fig. S33), which proved the remarkable configurational stability of the (*R*/*S*)-**4CzZ[6]CPP** macrocycle with a rigid chiral scaffold.

As shown in Fig. 5b, the CD and CPL spectra of (*R*/*S*)-**4CzZ[6]CPP** were recorded in toluene at 298 K. A perfect mirror-image Cotton effect was exhibited in the CD spectrum with three bands at 299, 334 and 367 nm, corresponding to the UV-vis spectrum. The short wavelength waves at 299 and 334 nm could be attributed to the n–π* and π–π* transitions of the CPP framework, and the strong CD signal at 367 nm could be assigned to the ICT transition process from 3,6-di-*tert*-butylcarbazole to the cyano-group in (*R*/*S*)-**4CzZ[6]CPP**. The intense CD signal at 334 nm showed a $|\Delta\varepsilon|$ value of 70.6 M^{-1} cm^{-1}, which showed the efficient transfer of the chiroptical response from the axially chiral unit to the entire π-conjugated CPP framework through electronic delocalization. Additionally, the maximum absorption dissymmetry factor of $|g_{abs}| = 5.4 \times 10^{-3}$ occurred at 367 nm, with corresponding values of 2.09×10^{-3} and 3.09×10^{-3} at 299 and 334 nm, respectively (Fig. 5c). The CPL spectra of *R*-**4CzZ[6]CPP** and *S*-**4CzZ[6]CPP** were measured in toluene at 298 K with a peak at 458 nm. Surprisingly, we observed intense CPL signals with high g_{lum} values of $+6.08 \times 10^{-3}$ for *R*-**4CzZ[6]CPP** and -6.43×10^{-3} for *S*-**4CzZ[6]CPP**, respectively (Fig. 5d), which ranked among the best reported chiral CPPs. The CPL spectra and g_{lum} values of *R*/*S*-**4CzZ[6]CPP** in DCM and film states were recorded in Fig. S24 and S23. Furthermore, **4CzZ[6]CPP** demonstrated an exceptional B_{CPL} of 344 M^{-1} cm^{-1}, representing, to the best of our knowledge, the highest reported value for chiral CPP derivatives produced by a chirality embedding strategy (Table S13).

In addition, we compared the chiral response signals of (*R*/*S*)-**AC** and (*R*/*S*)-**4CzZ[6]CPP**. Mirror-image chiral signals were observed in both the CD and CPL spectra of (*R*/*S*)-**AC** (Fig. S28), and moderate signals with g_{lum} values of $+2.60 \times 10^{-3}$ for *R*-**AC** and -2.40×10^{-3} for *S*-**AC** were observed, respectively (Fig. S29). Importantly, the $|g_{lum}|$ values of (*R*/*S*)-**4CzZ[6]CPP** exhibited a 2.5-fold enhancement compared with that of (*R*/*S*)-**AC**. This finding highlighted the crucial role of structural rigidity in amplifying the chiroptical response, and also provided experimental evidence for CPPs as a rigid chain to amplify g_{lum} values. This established *R*/*S*-**4CzZ[6]CPP** as a promising candidate for chiroptical applications, and

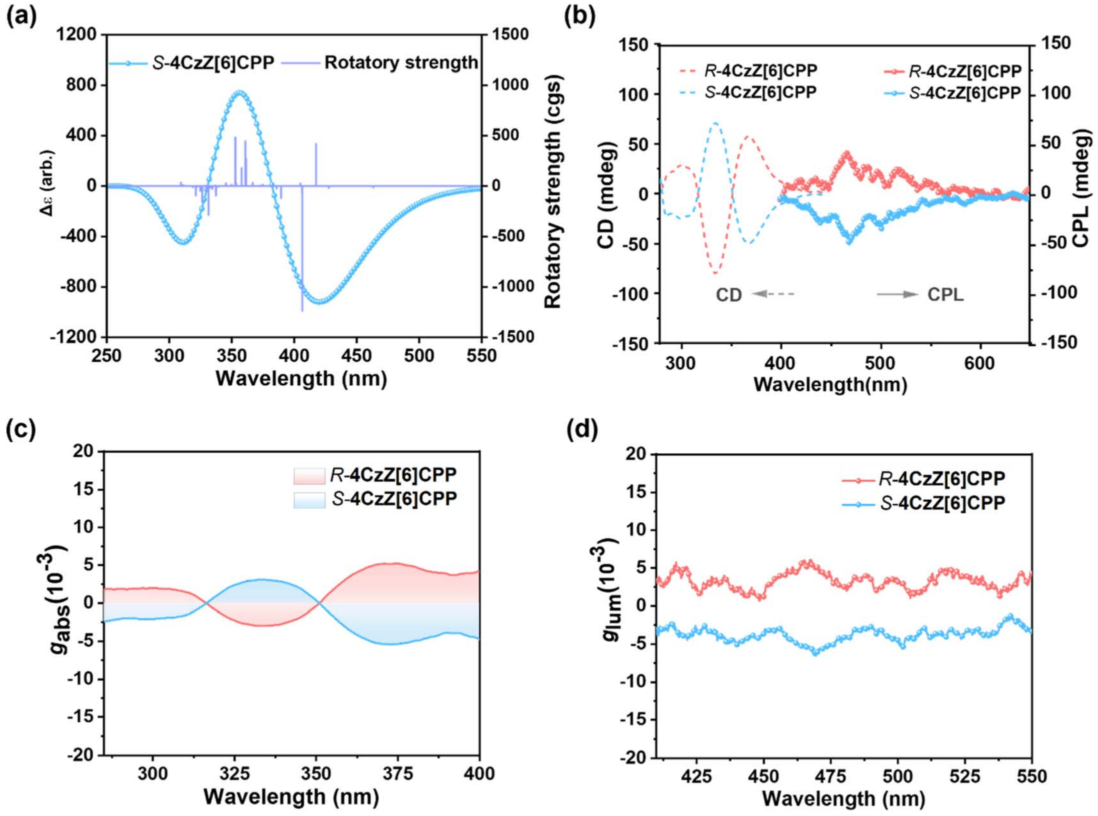

Fig. 5 (a) Calculated CD spectrum of *S*-4CzZ[6]CPP with the PBE1PBE/6-31 G (d, p) basis group. (b) The CD and CPL spectra of *R*/*S*-4CzZ[6]CPP and the corresponding (c) absorption and (d) photoluminescence asymmetry factor values.

provided a feasible design principle for developing advanced CPP-based luminescent materials.

In order to clarify how the g_{lum} value was amplified, we further conducted theoretical calculations under the same basis set (Fig. S38, S39 and Tables S11, S12). On the one hand, the μ values were 1.16×10^{-18} esu cm for *R*-**AC** and 0.90×10^{-18} esu cm for *R*-**4CzZ[6]CPP**, and the m values were 0.46×10^{-20} erg G^{-1} for *R*-**AC** and 0.50×10^{-20} erg G^{-1} for *R*-**4CzZ[6]CPP** for the $S_0 \rightarrow S_1$ transition, respectively. Furthermore, the $\cos\theta$ values were extremely close, being 0.97 and 0.99, respectively, thus yielding the theoretical g_{abs} value of 1.58×10^{-2} for *R*-**AC** and 2.19×10^{-2} for *R*-**4CzZ[6]CPP**. On the other hand, compared to *R*-**AC** with μ of 1.40×10^{-18} esu cm and m of 0.23×10^{-20} erg G^{-1}, *R*-**4CzZ[6]CPP** displayed a smaller μ of 1.23×10^{-18} esu cm, while possessing a larger m of 0.45×10^{-20} erg G^{-1} in the transition from the S_1 to S_0 state, and the $\cos\theta$ values were similar at 0.98 and 0.99. Consequently, *R*-**4CzZ[6]CPP** exhibited a larger g_{lum} of 1.41×10^{-2}, which was increased by 2.2-fold compared to *R*-**AC** with a g_{lum} of 0.65×10^{-2}. This result was consistent with the amplification factor observed in experiments, demonstrating that the introduction of a CPP structure led to a smaller μ, which facilitated the amplification of the chiroptical signals.

Conclusions

We designed an axially chiral intercalated CPP derivative modified with a D–A unit, named **4CzZ[6]CPP**, exhibiting bright blue emission at 458 nm. Single-crystal X-ray diffraction confirmed the bow-shaped structure, and the π-extended conjugation conferred a large molar extinction coefficient. Moreover, a charge transfer state was introduced to promote the radiation transition, and the molecular rigidity was enhanced by increasing the CPP size to limit non-radiative transitions. Both factors created a remarkable PLQY of 74.4%. Furthermore, the increased scaffold rigidity improved the enantiomer stability and constrained the rotation of the axially chiral unit, and thereby the chiroptical responses of (*R*/*S*)-**4CzZ[6]CPP** were amplified, achieving a maximum $|g_{\mathrm{lum}}|$ of 6.43×10^{-3}, which was a 2.5-fold enhancement compared to the axially chiral precursors. In addition, the results of theoretical calculations also proved the amplification effect. Based on the high PLQY and large g_{lum} value, an excellent CPL performance with a B_{CPL} of 344 M^{-1} cm^{-1} was obtained, which is the highest value reported for chiral CPPs constructed through a chirality embedding strategy, indicating that **4CzZ[6]CPP** is a promising candidate for advanced CPL materials. We believe that these results offer valuable design principles to construct chiral CPPs with efficient CPL emission for applications in optoelectronic materials and devices.

Author contributions

MXY and CFC designed the research and wrote the manuscript. MXY carried out the synthesis and characterization of all species, collected the crystallographic data and measured the photophysical properties and chiroptical properties. CF and WCG performed the DFT and TD-DFT calculations. All authors interpreted the results and contributed to reviewing and editing the manuscript.

Conflicts of interest

There are no conflicts to declare.

Data availability

CCDC 2422143 contains the supplementary crystallographic data for this paper.[26]

The supplementary data supporting the findings of this paper are included in the Supplementary Information (SI). Supplementary information (SI): detailed methods, experimental details and photophysical properties. See DOI: **https://doi.org/10.1039/d5sc07321a**.

Acknowledgements

We thank the National Natural Science Foundation of China (92256304) and the National Key Research and Development Program of China (2022YFA1204401) for the financial support.

References

1 (*a*) S. E. Lewis, *Chem. Soc. Rev.*, 2015, **44**, 2221–2304; (*b*) Q.-S. Deng, X.-W. Chen, X.-H. Yu, J.-F. Xing, B.-H. Zheng, G. Xiao, B. Zou and Y.-Z. Tan, *Angew. Chem., Int. Ed.*, 2025, **64**, e202506376; (*c*) J.-N. Gao, A. Bu, Y. Chen, M. Huang, Z. Chen, X. Li, C.-H. Tung, L.-Z. Wu and H. Cong, *Angew. Chem., Int. Ed.*, 2024, **63**, e202408016; (*d*) Y. Shi, C. Li, J. Di, Y. Xue, Y. Jia, J. Duan, X. Hu, Y. Tian, Y. Li, C. Sun, N. Zhang, Y. Xiong, T. Jin and P. Chen, *Angew. Chem., Int. Ed.*, 2024, **63**, e202402800; (*e*) X.-S. Du, D.-W. Zhang, Y. Guo, J. Li, Y. Han and C.-F. Chen, *Angew. Chem., Int. Ed.*, 2021, **60**, 13021–13028; (*f*) F. Zhang, X.-S. Du, D.-W. Zhang, Y.-F. Wang, H.-Y. Lu and C.-F. Chen, *Angew. Chem., Int. Ed.*, 2021, **60**, 15291–15295.

2 (*a*) X. Li, S. Guo and H. Jiang, *Chem. Commun.*, 2025, **61**, 9836–9852; (*b*) R. Jasti, J. Bhattacharjee, J. B. Neaton and C. R. Bertozzi, *J. Am. Chem. Soc.*, 2008, **130**, 17646–17647.

3 X.-W. Chen, Q.-S. Deng, B.-H. Zheng, J.-F. Xing, H.-R. Pan, X.-J. Zhao and Y.-Z. Tan, *J. Am. Chem. Soc.*, 2024, **146**, 31665–31670.

4 (*a*) S. Li, Z.-Y. Qiu, J.-S. Dang and H. Sakurai, *Chem. Commun.*, 2024, **60**, 6451–6454; (*b*) S. Wu, J. Jie, L. Liu, L. Liu, S. Guo, X. Li, J. He, Z. Lian, Y. Wang, X. Xu, H. Su, X. Chen and H. Jiang, *Angew. Chem., Int. Ed.*, 2025, e202512167; (*c*) L. Zhan, C. Dai, G. Zhang, J. Zhu, S. Zhang, H. Wang, Y. Zeng, C.-H. Tung, L.-Z. Wu and H. Cong, *Angew. Chem., Int. Ed.*, 2022, **61**, e202113334.

5 (*a*) W. Shi, Y. Hu, L. Leanza, Y. Shchukin, P. A. Hoffmann, M.-H. Li, C. Ning, Z.-Y. Cao, Y.-Q. Xu, P. Du, M. von Delius, G. M. Pavan and Y. Xu, *Angew. Chem., Int. Ed.*, 2025, **64**, e202421459; (*b*) N. Geue, M. Freiberger, S. Frühwald, A. Görling, T. Drewello and P. E. Barran, *J. Phys. Chem.*

Lett., 2024, **15**, 6805–6811; (*c*) X. Zhang, Y. Xu and P. Du, *Acc. Mater. Res.*, 2025, **6**, 399–410; (*d*) S.-Z. Guo, L. Liu, F. Su, H.-J. Yang, G.-Q. Liu, Y.-Q. Fan, J. He, Z. Lian, X.-N. Li, W.-J. Guo, X.-B. Chen and H. Jiang, *JACS Au*, 2024, **4**, 402–410.

6 J. Geng, *Adv. Opt. Photon*, 2013, **5**, 456–535.

7 (*a*) L. E. MacKenzie and R. Pal, *Nat. Rev. Chem.*, 2021, **5**, 109–124; (*b*) J. Li, Y. Guan, T.-T. Hao, J. Huang, Y. Chen, H. Li, P. Duan and H.-L. Xie, *Angew. Chem., Int. Ed.*, 2025, **64**, e202423395; (*c*) L. E. MacKenzie and R. Pal, *Nat. Rev. Chem.*, 2021, **5**, 109; (*d*) Y. Zhou, C. Lu, Z. Lu, Z. Guo, C. Ye, V. V. Tsukruk and R. Xiong, *Small*, 2023, **19**, 2303064; (*e*) M.-J. Ji, W.-L. Zhao, M. Li and C.-F. Chen, *Nat. Commun.*, 2025, **16**, 2940; (*f*) S. Jia, B. Yang, Y. Xie, T. Tao, J. Du, L. Yu, Y. Zhang, J. Zhang, W. Tang and J. Gong, *Adv. Funct. Mater.*, 2024, **34**, 2410206; (*g*) S. Jia, B. Yang, J. Du, J. Zhang, Y. Xie, T. Tao, J. Tang, W. Tang and J. Gong, *Small*, 2025, **21**, 2408219.

8 W.-L. Zhao, W.-C. Guo, K. K. Tan, Z.-X. Yu, M. Li and C.-F. Chen, *Angew. Chem., Int. Ed.*, 2025, **64**, e202416863.

9 Q. Wang, J. Bao, Y. Zhang, Y. Wang, D. Qiu, J. Yang, J. Zhang, H. Gao, Y. Wu, H. Dong, H. Yang and Z. Wei, *Adv. Mater.*, 2024, **36**, 2312396.

10 (*a*) G. Li, L.-L. Mao, J.-N. Gao, X. Shi, Z.-Y. Huo, J. Yang, W. Zhou, H. Li, H.-B. Yang, C.-H. Tung, L.-Z. Wu and H. Cong, *Angew. Chem., Int. Ed.*, 2025, **64**, e202419435; (*b*) W. Zhang, J. Wang, X. Zhang, B. Yuan, P. Fang, N. Yin and P. Du, *Angew. Chem., Int. Ed.*, 2025, **64**, e202508017; (*c*) S. Tan, Y.-Q. Han, G. Wang, L. Chen, L. Shao, M. Xiao, B. Zhao, F. Huang and B. Hua, *Angew. Chem., Int. Ed.*, 2025, e202508361; (*d*) K. Lan, C. Zhang, Y. Li, C. Hu, Z. Su and C. Cheng, *Angew. Chem., Int. Ed.*, 2025, e202507763; (*e*) S. Tan, Y.-Q. Han, G. Wang, L. Chen, L. Shao, M. Xiao, B. Zhao, F. Huang and B. Hua, *Angew. Chem., Int. Ed.*, 2025, e202508361.

11 S. Hitosugi, W. Nakanishi, T. Yamasaki and H. Isobe, *Nat. Commun.*, 2011, **2**, 492.

12 J. Wang, G. Zhuang, Q. Huang, Y. Xiao, Y. Zhou, H. Liu and P. Du, *Chem. Commun.*, 2019, **55**, 9456–9459.

13 J. Wang, H. Shi, S. Wang, X. Zhang, P. Fang, Y. Zhou, G.-L. Zhuang, X. Shao and P. Du, *Chem.–Eur. J.*, 2022, **28**, e202103828.

14 A. Li, X. Zhang, S. Wang, K. Wei and P. Du, *Org. Lett.*, 2023, **25**, 1183–1187.

15 X. Kong, X. Zhang, B. Yuan, W. Zhang, D. Lu and P. Du, *J. Org. Chem.*, 2024, **89**, 8255–8261.

16 Q. Huang, J. Zhang, H. Chen, X. Kong, P. Xu and P. Du, *Org. Chem. Front.*, 2023, **10**, 911–915.

17 Y. Wu, G. Zhuang, S. Cui, Y. Zhou, J. Wang, Q. Huang and P. Du, *Chem. Commun.*, 2019, **55**, 14617–14620.

18 J. Malinčík, S. Gaikwad, J. P. Mora-Fuentes, M.-A. Boillat, A. Prescimone, D. Häussinger, A. G. Campaña and T. Šolomek, *Angew. Chem., Int. Ed.*, 2022, **61**, e202208591.

19 S. Guo, L. Liu, X. Li, G. Liu, Y. Fan, J. He, Z. Lian, H. Yang, X. Chen and H. Jiang, *Small*, 2024, **20**, 2308429.

20 Y. Segawa, A. Fukazawa, S. Matsuura, H. Omachi, S. Yamaguchi, S. Irle and K. Itami, *Org. Biomol. Chem.*, 2012, **10**, 5979–5984.

21 (*a*) K. Takaishi, S. Murakami, F. Yoshinami and T. Ema, *Angew. Chem., Int. Ed.*, 2022, **61**, e202204609; (*b*) W. Huang, Y. Zhu, K. Zhou, L. Chen, Z. Zhao, E. Zhao and Z. He, *Chem.–Eur. J.*, 2024, **30**, e202303667.

22 (*a*) M. Li, Y.-F. Wang, D. Zhang, L. Duan and C.-F. Chen, *Angew. Chem., Int. Ed.*, 2020, **59**, 3500–3504; (*b*) K.-K. Tan, D.-W. Zhang, W.-L. Zhao, M. Li and C.-F. Chen, *Chem. Eng. J.*, 2023, **462**, 142123.

23 (*a*) P. Chen, X. Yin, N. Baser-Kirazli and F. Jäkle, *Angew. Chem., Int. Ed.*, 2015, **54**, 10768–10772; (*b*) J.-F. Chen, X. Yin, B. Wang, K. Zhang, G. Meng, S. Zhang, Y. Shi, N. Wang, S. Wang and P. Chen, *Angew. Chem., Int. Ed.*, 2020, **59**, 11267–11272; (*c*) F. Zhao, J. Zhao, H. Liu, Y. Wang, J. Duan, C. Li, J. Di, N. Zhang, X. Zheng and P. Chen, *J. Am. Chem. Soc.*, 2023, **145**, 10092–10103.

24 T. Iwamoto, Y. Watanabe, Y. Sakamoto, T. Suzuki and S. Yamago, *J. Am. Chem. Soc.*, 2011, **133**, 8354–8361.

25 (*a*) E. Kayahara, V. K. Patel and S. Yamago, *J. Am. Chem. Soc.*, 2014, **136**, 2284–2287; (*b*) E. R. Darzi and R. Jasti, *Chem. Soc. Rev.*, 2015, **44**, 6401–6410.

26 CCDC 2422143: Experimental Crystal Structure Determination, 2025, DOI: **10.5517/ccdc.csd.cc2m9fn1**.